



Differentiation of high-grade from low-grade diffuse gliomas using diffusion-weighted imaging: a comparative study of mono-, bi-, and stretched-exponential diffusion models

Masaaki Kusunoki¹ · Kazufumi Kikuchi¹ · Osamu Togao¹ · Koji Yamashita¹ · Daichi Momosaka¹ · Yoshitomo Kikuchi¹ · Daisuke Kuga² · Nobuhiro Hata² · Masahiro Mizoguchi² · Koji Iihara² · Satoshi O. Suzuki³ · Toru Iwaki³ · Yuta Akamine⁴ · Akio Hiwatashi⁵

Received: 8 February 2020 / Accepted: 5 May 2020 / Published online: 18 May 2020
© The Author(s) 2020

Abstract

Purpose Diffusion-weighted imaging (DWI) plays an important role in the preoperative assessment of gliomas; however, the diagnostic performance of histogram-derived parameters from mono-, bi-, and stretched-exponential DWI models in the grading of gliomas has not been fully investigated. Therefore, we compared these models' ability to differentiate between high-grade and low-grade gliomas.

Methods This retrospective study included 22 patients with diffuse gliomas (age, 23–74 years; 12 males; 11 high-grade and 11 low-grade gliomas) who underwent preoperative 3 T-magnetic resonance imaging from October 2014 to August 2019. The apparent diffusion coefficient was calculated from the mono-exponential model. Using 13 *b*-values, the true-diffusion coefficient, pseudo-diffusion coefficient, and perfusion fraction were obtained from the bi-exponential model, and the distributed-diffusion coefficient and heterogeneity index were obtained from the stretched-exponential model. Region-of-interests were drawn on each imaging parameter map for subsequent histogram analyses.

Results The skewness of the apparent diffusion, true-diffusion, and distributed-diffusion coefficients was significantly higher in high-grade than in low-grade gliomas (0.67 ± 0.67 vs. -0.18 ± 0.63 , 0.68 ± 0.74 vs. -0.08 ± 0.66 , 0.63 ± 0.72 vs. -0.15 ± 0.73 ; $P = 0.0066$, 0.0192 , and 0.0128 , respectively). The 10th percentile of the heterogeneity index was significantly lower (0.77 ± 0.08 vs. 0.88 ± 0.04 ; $P = 0.0004$), and the 90th percentile of the perfusion fraction was significantly higher (12.64 ± 3.44 vs. $7.14 \pm 1.70\%$; $P < 0.0001$), in high-grade than in low-grade gliomas. The combination of the 10th percentile of the true-diffusion coefficient and 90th percentile of the perfusion fraction showed the best area under the receiver operating characteristic curve (0.96).

Conclusion The bi-exponential model exhibited the best diagnostic performance for differentiating high-grade from low-grade gliomas.

Keywords High-grade glioma · Low-grade glioma · Diffusion-weighted imaging · Bi-exponential model · Stretched-exponential model

Electronic supplementary material The online version of this article (<https://doi.org/10.1007/s00234-020-02456-2>) contains supplementary material, which is available to authorized users.

✉ Kazufumi Kikuchi
kkikuchi@radiol.med.kyushu-u.ac.jp

¹ Department of Clinical Radiology, Graduate School of Medical Sciences, Kyushu University, 3-1-1 Maidashi, Higashi-ku, Fukuoka 812-8582, Japan

² Department of Neurosurgery, Graduate School of Medical Sciences, Kyushu University, 3-1-1 Maidashi, Higashi-ku, Fukuoka 812-8582, Japan

³ Department of Neuropathology, Graduate School of Medical Sciences, Kyushu University, 3-1-1 Maidashi, Higashi-ku, Fukuoka 812-8582, Japan

⁴ Philips Japan, 13-37, Kohnan 2-chome, Minato-ku, Tokyo 108-8507, Japan

⁵ Department of Molecular Imaging & Diagnosis, Graduate School of Medical Sciences, Kyushu University, 3-1-1 Maidashi, Higashi-ku, Fukuoka 812-8582, Japan

Introduction

Gliomas are the most common primary intracranial neoplasms and have various histological grades that reflect malignancy or aggressiveness, according to the World Health Organization (WHO) classification [1]. Distinguishing high-grade gliomas (HGGs; grades III and IV) from low-grade gliomas (LGGs; grades I and II) is important, as their prognoses and therapeutic strategies differ. HGGs are usually treated surgically, followed by concurrent radiation and chemotherapy [2]. HGGs misdiagnosed as LGGs are treated less aggressively than necessary, and vice versa. Therefore, differentiating glioma types before initiating treatment is desirable.

Diffusion-weighted imaging (DWI) provides useful imaging biomarkers for grading gliomas, enabling the quantitative assessment of tumor characteristics without tracer injections. The apparent diffusion coefficient (ADC), which is a useful biomarker reflecting cellular density, is conventionally calculated using two b -values (0 and 1000 s/mm²) [3]. It has good diagnostic performance in differentiating HGGs from LGGs [3], but there is substantial overlap [4, 5]. Using the ADC in the differential diagnosis may be an oversimplification; it assumes that the only underlying mechanism of observed signal decay is the diffusive motion of water molecules.

Le Bihan et al. [6] proposed using the intravoxel incoherent motion (IVIM) to simultaneously measure perfusion and diffusion. At low b -values, the intravoxel motion of water molecules in *in vivo* tissues is greatly influenced by the microcirculation of blood capillaries (perfusion), whereas at high b -values, true diffusive motion predominates, resulting in bi-exponential signal decay. The bi-exponential model for IVIM imaging is useful for differentiating HGGs and LGGs in adults and children [7–9]. Additionally, Bennett et al. introduced the stretched-exponential model [10] to incorporate multicomponent intravoxel diffusion, which leads to non-exponential signal decay. This model enables the measurement of the water diffusion heterogeneity index α , which ranges from 0 to 1 (a value of 1 indicates water diffusion). Accumulating evidence suggests that stretched-exponential DWI is useful for assessing gliomas [11–16] and other tumors, including breast [17], pancreatic [18], hepatic [19], prostate [20], bladder [21], and renal cancers [22].

Histogram analysis is a quantitative technique that has been used for grading gliomas [23, 24]. Kang et al. suggested that histogram-derived ADC values of the whole tumor volume were useful for grading gliomas, while a single ADC value of the regional region-of-interest (ROI) might not effectively reflect the heterogeneous nature of gliomas [24]. To date, two studies [13, 14] have compared the diagnostic performance of mono-, bi-, and stretched-exponential DWI for grading gliomas, using mean ROI values. To the best of our knowledge, a histogram analysis has not been applied to this particular problem.

Therefore, the purpose of this study was to compare the imaging parameters obtained from mono-, bi-, and stretched-exponential DWI models for differentiating HGGs from LGGs.

Methods

This retrospective study was approved by our Institutional Review Board, and the requirement for informed consent was waived.

Patients

The initial population of 66 patients (55 HGGs and 11 LGGs) met the following inclusion criteria: (1) consecutive patients with histopathologically proven gliomas between October 2014 and August 2019; (2) MRI scans that had been performed within 2 weeks before surgery; (3) patients who had not undergone surgical treatment at the time of the first MRI; and (4) patients for whom the 13 b -values of diffusion imaging were acquired. Of the 66 patients, 44 were excluded to create a cohort of equal numbers of consecutive HGG and LGG patients (for statistical simplicity as well as preventing bias from overrepresentation of HGGs; all data [$N=55$ HGG patients] is shown in Online Resources 4 and 5). In total, 22 patients, including 11 consecutive patients with HGGs (range, median age; 31–71, 65 years; 4 males and 7 females) treated from June 2018 to October 2018, and 11 with LGGs (23–74, median age; 45 years; 8 males and 3 females), were enrolled from October 2014 to August 2019. The inclusion and exclusion criteria are summarized in Online Resource 1. The period of enrollment differed between patients with HGGs and LGGs, since we included the most recent 11 consecutive patients with HGGs.

Histopathologic diagnosis

The patients' demographics and pathological diagnoses, based on the 2016 WHO classification [1], are as follows: the 11 HGGs included 7 glioblastomas (isocitrate dehydrogenase (IDH)-wild type; WHO grade IV; age, 48–71 years; 3 males and 4 females); 1 diffuse midline glioma (H3 K27M-mutant type; WHO grade III; age, 31 years; female); 2 anaplastic astrocytomas (IDH-mutant type; WHO grade III; age, 32 and 71 years; 1 male and 1 female); and 1 anaplastic oligodendroglioma (IDH-mutant type; WHO grade III; age, 47 years; female). The 11 LGGs included 5 diffuse astrocytomas (IDH-mutant type; WHO grade II; age, 23–45 years; 4 males and 1 female); 4 diffuse astrocytomas (IDH-wild type; WHO grade II; age, 29–74 years; 3 males and 1 female); and 2 oligodendrogliomas (IDH-mutant type, WHO grade II; age, 49 and 73 years; 1 male and 1 female).

MRI

MRI was performed as previously described [9] using 3 T MR scanners (Achieva 3.0 T TX or Ingenia 3.0 T CX; Philips Healthcare, Best, The Netherlands) with 8- or 15-channel head coils. DWI was obtained in the axial plane using a two-dimensional single-shot spin-echo echo-planar imaging diffusion sequence. We used 13 b -values (0, 10, 20, 30, 50, 80, 100, 200, 300, 400, 600, 800, and 1000 s/mm²) in three orthogonal directions. At our institution, preoperative imaging of patients with brain tumors routinely uses the same 13 b -values. The other MRI parameters were as follows: repetition time/echo time, 2500/70 ms; matrix, 128 × 126 (reconstructed to 256 × 256); number of excitations, 1; section thickness/gap, 5/1 mm; FOV, 230 × 230 mm²; number of sections, 11; sensitivity encoding factor, 1.5; and total scan time, 2 m 7 s. Standard MR sequences (T1-, and T2-weighted images, fluid attenuated inversion recovery, and contrast-enhanced T1-weighted images) were obtained for diagnostic purposes. DWI was acquired before contrast agent injection. Imaging data were used for mono-, bi-, and stretched-exponential DWI models for subsequent image analysis. No denoising or co-registration for the DWI data were performed before analysis.

Image analysis

From the acquired images, model fitting was performed using image analyzer software (diffusion analysis software, EXPRESS 2.0; Philips Healthcare) [25]. The mono-exponential DWI provides the ADC values using the formula:

$$\frac{SI_{1000}}{SI_0} = \exp(-b \times ADC) \quad (1)$$

where SI_0 corresponds to the signal intensity without diffusion weighting ($b = 0$ s/mm²) and SI_{1000} is the signal intensity at $b = 1000$ s/mm². For bi-exponential DWI data analysis, the bi-exponential model was defined by the following equation:

$$\frac{SI_b}{SI_0} = f \times \exp(-b \times D^*) + (1-f) \times \exp(-b \times D) \quad (2)$$

where SI_b is the signal intensity acquired with different b -values, f is the perfusion fraction, D^* is the pseudo-diffusion coefficient, and D is the true-diffusion coefficient. The bi-exponential DWI model is based on the fit of three parameters. First, the D was determined from data with higher b -values ($b = 300, 400, 600, 800,$ and 1000 s/mm²). When high b -values were used and the IVIM component was negligible, the following least-squares curve fit was used:

$$\frac{SI_b}{SI_0} = \exp(-b \times D) \quad (3)$$

Second, the segmented method was used to calculate f according to the following equation:

$$f = (SI_0 - SI_{inter})/SI_0 \quad (4)$$

Here, SI_{inter} is the intersection point of the y -axis and line through $\ln SI_{300}$ and $\ln SI_{1000}$. Third, D^* was derived from the mono-exponential fit to Eq. (2).

The stretched-exponential DWI model is defined as follows:

$$\frac{SI_b}{SI_0} = \exp\{-(b \times DDC)^\alpha\} \quad (5)$$

where DDC is the distributed-diffusion coefficient, and α is the heterogeneity index. All 13 b -values were used to provide the best-fit parameter values for DDC and α simultaneously.

Two radiologists carefully evaluated each image on consensus, identified the T2-prolonged region where tumors existed, and drew ROIs on each tumor map for subsequent analysis. We used the single maximum section of each tumor for the ROI analysis. When placing the ROIs for each map, we carefully avoided cortical gray matter, which affects the f value. ROIs were copied on each parameter map to obtain pixel-by-pixel values for histogram analyses. The 10th, 25th, 50th (median), 75th, and 90th percentiles, as well as the mean, skewness, and kurtosis, of each parameter were recorded from the histograms. Note that our definition of an ROI may include edematous or necrotic regions within the tumor.

Statistical analysis

The percentiles, as well as the mean, skewness, and kurtosis of each parameter (i.e., ADC, D , D^* , f , DDC, and α), were compared between HGGs and LGGs using the Mann-Whitney U test. The diagnostic performance of each model parameter was evaluated by receiver operating characteristic (ROC) curve analysis. Combinations of two parameters from bi- and stretched-exponential DWI models were also assessed. Two independent areas under the curves (AUCs) were compared using the method developed by Delong et al. [26]. All statistical analyses were performed using commercial software programs (JMP, version 14.0.0; SAS Institute, Cary, NC, USA; Prism 7.0, GraphPad Software, La Jolla, CA, USA). P values < .05 were considered statistically significant.

Results

Histogram analysis

Figure 1 shows the normalized histograms of each parameter over all pixels in tumor ROIs. The ADC, D , DDC, and α from HGGs all exhibited a slight leftward shift (“+” skewness)

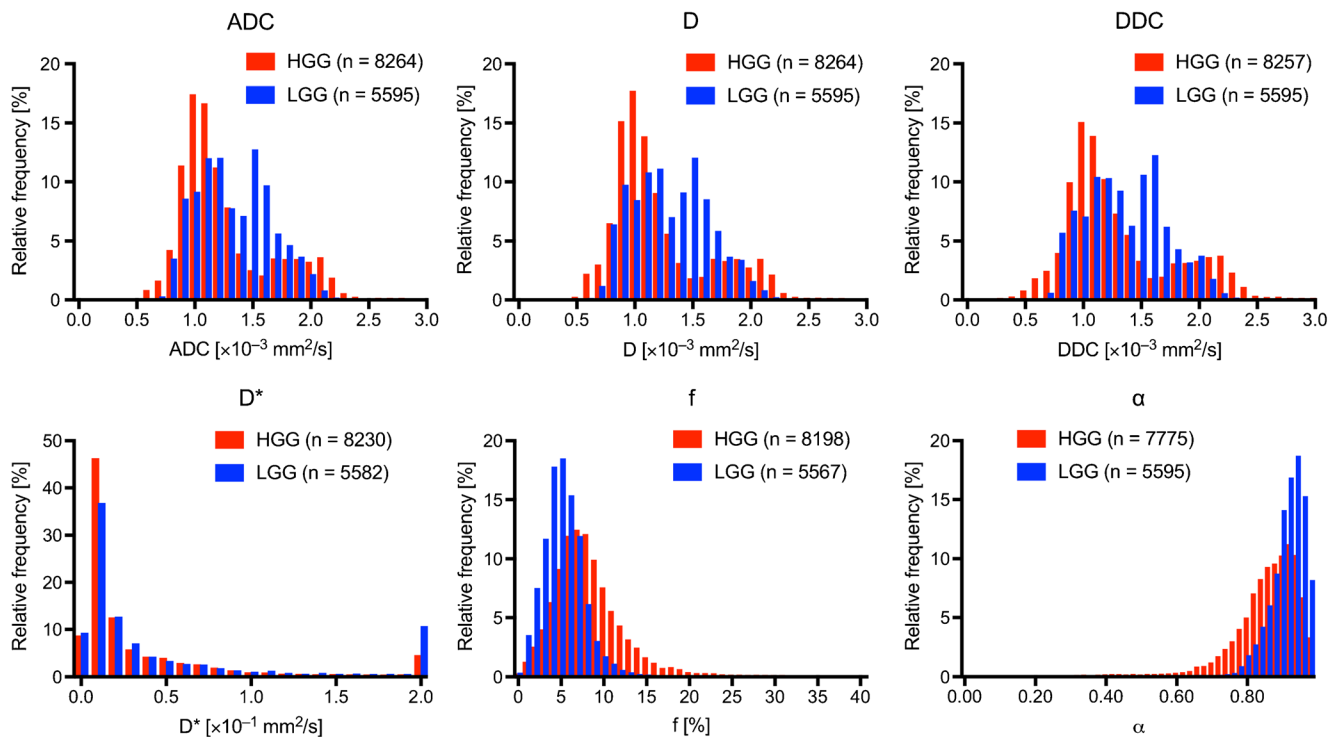


Fig. 1 Normalized histograms of each parameter Diffusion-related parameters (ADC, D, and DDC) and the heterogeneity index α from HGGs exhibit a slight leftward shift (“+” skewness) relative to those from LGGs, while the f from HGGs shows a slight rightward shift (“-” skewness) relative to that from LGGs. There is no difference in the D^* between

the two types of gliomas. α heterogeneity index, ADC apparent diffusion coefficient, D true-diffusion coefficient, DDC distributed diffusion coefficient, D^* pseudo-diffusion coefficient, f perfusion fraction, HGG high-grade diffuse glioma, LGG low-grade diffuse glioma

relative to those from LGGs, while the f from HGGs showed a slight rightward shift (“-” skewness) relative to that from LGGs. No significant difference in D^* between the two types of gliomas was observed.

Differentiation of HGGs and LGGs using parameter measurements

Table 1 shows the parameter measurements in the HGGs and LGGs. The 10th, 25th, 50th, 75th, and 90th percentiles of each parameter, as well as skewness and kurtosis, were all recorded from the histograms; the most useful values of each parameter are shown in Table 1. The entire set of our results can be found in Online Resource 2. For diffusion-related parameters, the skewness of ADC (ADC_{skw}), D_{skw} , and DDC_{skw} were significantly higher in HGGs than in LGGs (0.67 ± 0.67 vs. -0.18 ± 0.63 , 0.68 ± 0.74 vs. -0.08 ± 0.66 , 0.63 ± 0.72 vs. -0.15 ± 0.73 ; $P=0.007$, 0.002 , and 0.01 , respectively). The 10th percentile of α (α_{10}) was significantly lower in HGGs than in LGGs (0.77 ± 0.08 vs. 0.88 ± 0.04 ; $P < 0.001$). The 90th percentile of the perfusion fraction (f_{90}) was significantly higher in HGGs than that in LGGs (12.64 ± 3.44 vs. $7.14 \pm 1.70\%$; $P < 0.001$). There was no significant difference in D^* for differentiating between the two groups of gliomas ($P=0.30$ in the kurtosis of D^*).

ROC analysis

Table 2 shows the diagnostic performance and most useful values of the investigated parameters in differentiating HGGs and LGGs. The entire set of our results can be found in Online Resource 3. In the single-parameter analysis, the f_{90} showed one of the highest diagnostic performances (AUC = 0.96), with an optimal diagnosis

Table 1 Comparison of parameters between high- and low-grade diffuse gliomas

Parameters	High-grade glioma	Low-grade glioma	P value
ADC_{skw}	0.67 (0.22–1.12)	-0.18 (-0.60–0.24)	0.007 ^a
D_{skw}	0.68 (0.18–1.18)	-0.08 (-0.52–0.37)	0.02 ^a
DDC_{skw}	0.63 (0.15–1.12)	-0.15 (-0.64–0.33)	0.01 ^a
α_{10}	0.77 (0.72–0.83)	0.88 (0.86–0.91)	<0.001 ^a
D^*_{kur}	12.85 (-1.69–27.40)	13.13 (-5.09–31.35)	0.30 ^a
f_{90} (%)	12.64 (10.33–14.95)	7.14 (6.00–8.28)	<0.001 ^a

Data are expressed as mean values and 95% confidence intervals

α heterogeneity index, ADC apparent diffusion coefficient, D true-diffusion coefficient, D^* pseudo-diffusion, DDC distributed-diffusion coefficient, f perfusion fraction, kur kurtosis, skw skewness

^a Mann-Whitney U test

Table 2 Diagnostic performance of parameters in differentiating between high- and low-grade diffuse gliomas

Parameters	Sensitivity (%)	Specificity (%)	Accuracy (%)	Positive predictive value (%)	Negative predictive value (%)	Cutoff value	AUC
ADC_{skw}	72.7	90.9	81.8	88.9	76.9	> 0.38	0.83
D_{skw}	63.6	90.9	77.3	87.5	71.4	> 0.66	0.79
D^*_{skw}	81.8	54.6	68.2	64.3	75.0	> 1.50	0.62
$f90$ (%)	100	90.9	95.5	91.7	100	> 9.1	0.96
DDC_{skw}	63.6	90.9	77.3	87.5	71.4	> 0.48	0.81
$\alpha10$	81.8	90.9	86.4	90.0	83.3	≤ 0.85	0.91
$D10 + f90$	100	90.9	95.5	91.7	100	≤ 0.87 , > 9.1	0.96
$DDC_{skw} + \alpha10$	81.8	90.9	86.4	90.0	83.3	≤ -0.64 , ≤ 0.76	0.93

α heterogeneity index, ADC apparent diffusion coefficient, AUC area under the curve, D true-diffusion coefficient, D^* pseudo-diffusion coefficient, DDC distributed-diffusion coefficient, f perfusion fraction

cutoff value of 9.1%. The $\alpha10$ also showed good diagnostic performance (AUC = 0.91, cutoff value 0.85).

In the combined-parameters analysis, the combination of the $D10$ and $f90$ from the bi-exponential DWI model also showed one of the highest diagnostic performances (AUC = 0.96, cutoff values 0.87×10^{-3} mm²/s and 9.1% for $D10$ and $f90$, respectively). The combination of the DDC_{skw} and $\alpha10$ from the stretched-exponential DWI model exhibited good diagnostic performance (AUC = 0.93, cutoff values -0.64 and 0.76 for DDC_{skw} and $\alpha10$, respectively); however, no significant differences were detected between these combinations ($D10 + f90$, $DDC_{skw} + \alpha10$) and $f90$ ($P = 1.000$, 0.2059 , respectively) or $\alpha10$ ($P = 0.2894$, 0.6603 , respectively).

Figures 2 and 3 show representative images from patients with grades IV (glioblastoma) and II (oligodendroglioma) gliomas, respectively.

Discussion

We examined histogram-based parameters from mono-, bi-, and stretched-exponential DWI models to compare their diagnostic performance in distinguishing HGGs from LGGs. The ADC_{skw} , D_{skw} and DDC_{skw} were found to be useful diffusion parameters, providing good sensitivity and moderate specificity. Previous reports revealed that the ADC correlates well with cell density [27, 28]. Dense cells provide greater restriction of water movement, presumably due to increased cell membranes and intracellular space fraction. Accordingly, ADC measurements have been utilized to assess cell density in various tumors. The ADC calculated from two b -values (0 and 1000 s/mm²) decreases with glioma grade based on their histological features, including cell proliferation [29–31]. In the bi-exponential model, D was fitted only using high b -values, while the ADC and DDC were not. Therefore, D

reflects cell density more effectively than ADC and DDC by eliminating the effect of perfusion. The fast blood flow of the microcirculation observed at low b -values would yield slightly higher ADC and DDC values relative to the D value, as seen in our results. Furthermore, skewness represents a measure of asymmetry of the probability distribution. If a histogram has an elongated tail on the left side of the mean, it is negatively skewed; conversely, if a histogram has an elongated tail on the right side of the mean, it is positively skewed. In the present study, diffusion-related parameters from HGGs exhibited a slight leftward shift, meaning they were positively skewed. Therefore, HGGs had a greater frequency of pixels with lower diffusion-related parameters than the mean, compared with LGGs. While various components, such as edematous and necrotic tissues, exist within the HGGs, the result indicates the presence of more regions of higher density cells (i.e., tumor cells), showing the asymmetric leftward shift of the histograms. King et al. [32] revealed that there is a significant intra-treatment decrease in skewness in patients with head and neck squamous cell carcinomas. Our diffusion parameter results are consistent with those of previous studies [8, 9, 32].

The D^* was not helpful in glioma grading, as reported previously [8, 9, 33]. The D^* is a parameter of the fast component of the bi-exponential model and is sensitive to glioma microcirculation. Its poor reproducibility could be due to cardiac motion [34]. Cardiac-gating techniques may improve D^* assessment in tumors [35].

Our results indicated that a high percentile of f (i.e., $f90$) from the bi-exponential model is a powerful imaging biomarker for differentiating HGGs from LGGs. One aspect of glioma malignancy is angiogenesis, a key feature of the histopathological assessment in the WHO grading system. In the bi-exponential model, the fast component at low b -values is assumed to reflect the blood flow of the microcirculation, while the slow component at high b -values is governed by

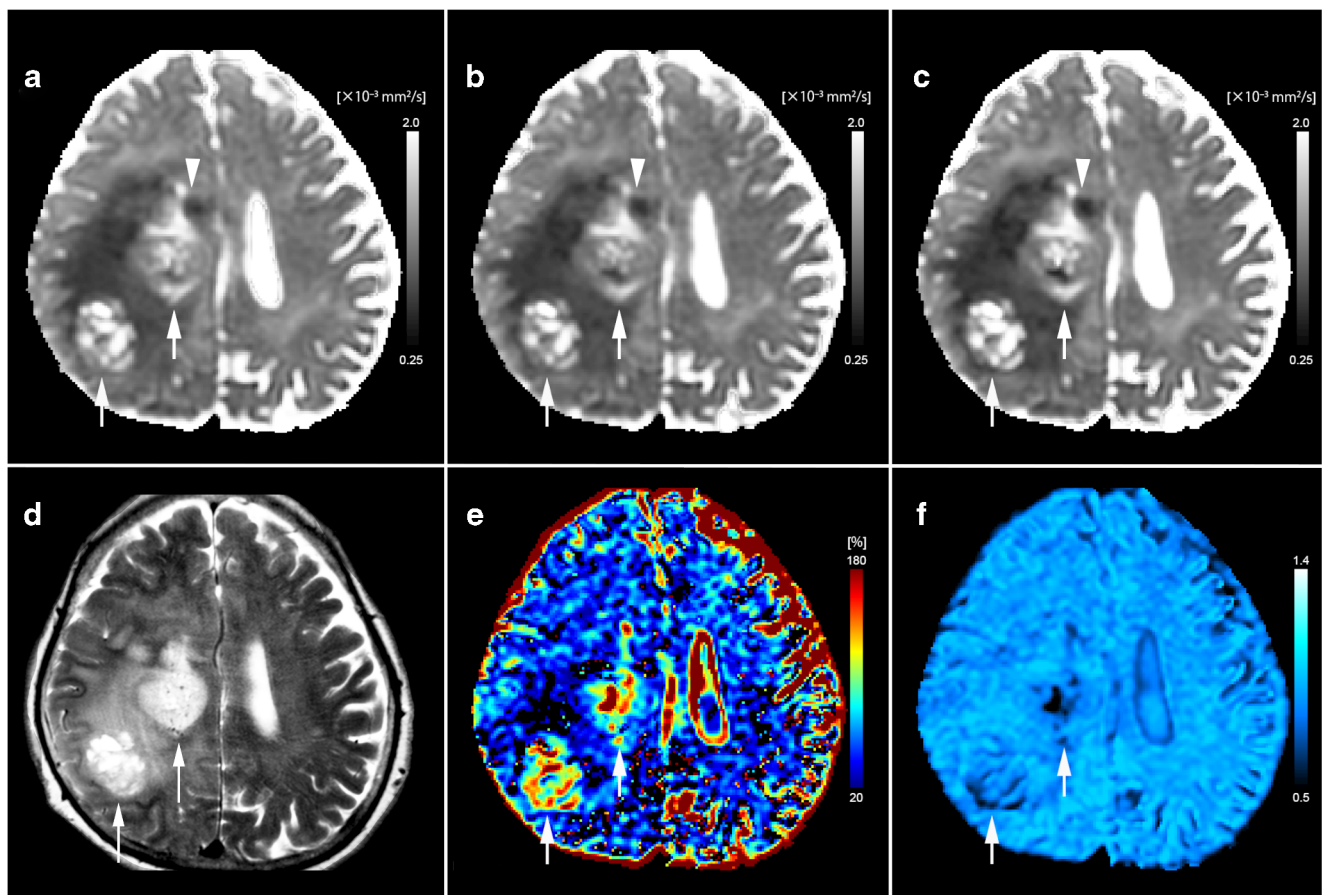


Fig. 2 Images from a 70-year-old woman with histologically proven glioblastoma, IDH-wild type (WHO grade IV). Diffusion-related coefficient maps show heterogeneous masses of low values (**a** ADC map; **b** D map; **c** DDC map; 0.79, 0.63, $0.60 \times 10^{-3} \text{ mm}^2/\text{s}$, respectively) in the right parietal lobe and centrum semiovale (arrows). There is a substantial restricted diffusion in the right frontal deep white matter (arrowheads). **d**

The T2-weighted image shows heterogeneously hyperintense foci in the mass. **e** The f map shows a high value (15.6%) in the lesion. **f** The α map shows a low value (0.65) in the lesion. α heterogeneity index, ADC apparent diffusion coefficient, D true-diffusion coefficient, DDC distributed diffusion coefficient, f perfusion fraction, IDH isocitrate dehydrogenase, WHO World Health Organization

the pure diffusive motion of water molecules. The f_{90} of HGGs was significantly higher than that of LGGs, in agreement with previous studies [7–9, 36]. However, Bai et al. reported that the f was significantly lower in HGGs than in LGGs [13], which contradicts our results. Further investigations are needed to resolve this issue.

A low percentile of the heterogeneity index α (i.e., α_{10}) from the stretched-exponential model is also useful for differentiating HGGs from LGGs. The α measures how much the signal decay deviates from the mono-exponential decay within a voxel. A value of α close to one indicates high homogeneity in apparent diffusion. Lower values of α indicate high heterogeneity, namely, the multiple-component decay from multiple-apparent diffusion of water molecules. In the WHO glioma grading system, HGGs require the presence of histopathological features such as anaplasia of glial cells, mitotic activity, and microvascular proliferation and/or necrosis, while LGGs require at most cytological atypia alone [1]. Therefore, HGGs would include more distinct structural

components within the voxel and are microscopically more heterogeneous than are LGGs, providing lower values of α . Few studies have applied the α to brain tumors. Kwee et al. demonstrated that the α of HGGs is significantly different from that of normal brain structures [11]. Other studies showed that the α of HGGs is significantly lower than that of LGGs [13, 14, 16], consistent with our findings.

In the combined-parameters analysis, the combination of the D_{10} and f_{90} showed the best diagnostic performance of all the parameters investigated in our study. In combination, these two parameters can be used to evaluate different pathologic features, vascularity, and cell density in gliomas. Some glioblastomas exhibit high vascularity and low cell density due to intratumoral necrosis. Thus, the bi-exponential DWI model is particularly useful in such cases because it can simultaneously evaluate both, as well as perfusion parameters, in the same anatomical space, which provides an advantage over the single-parameter analysis of the mono-exponential model. Although the AUC value for the combined DDC_{skw} and

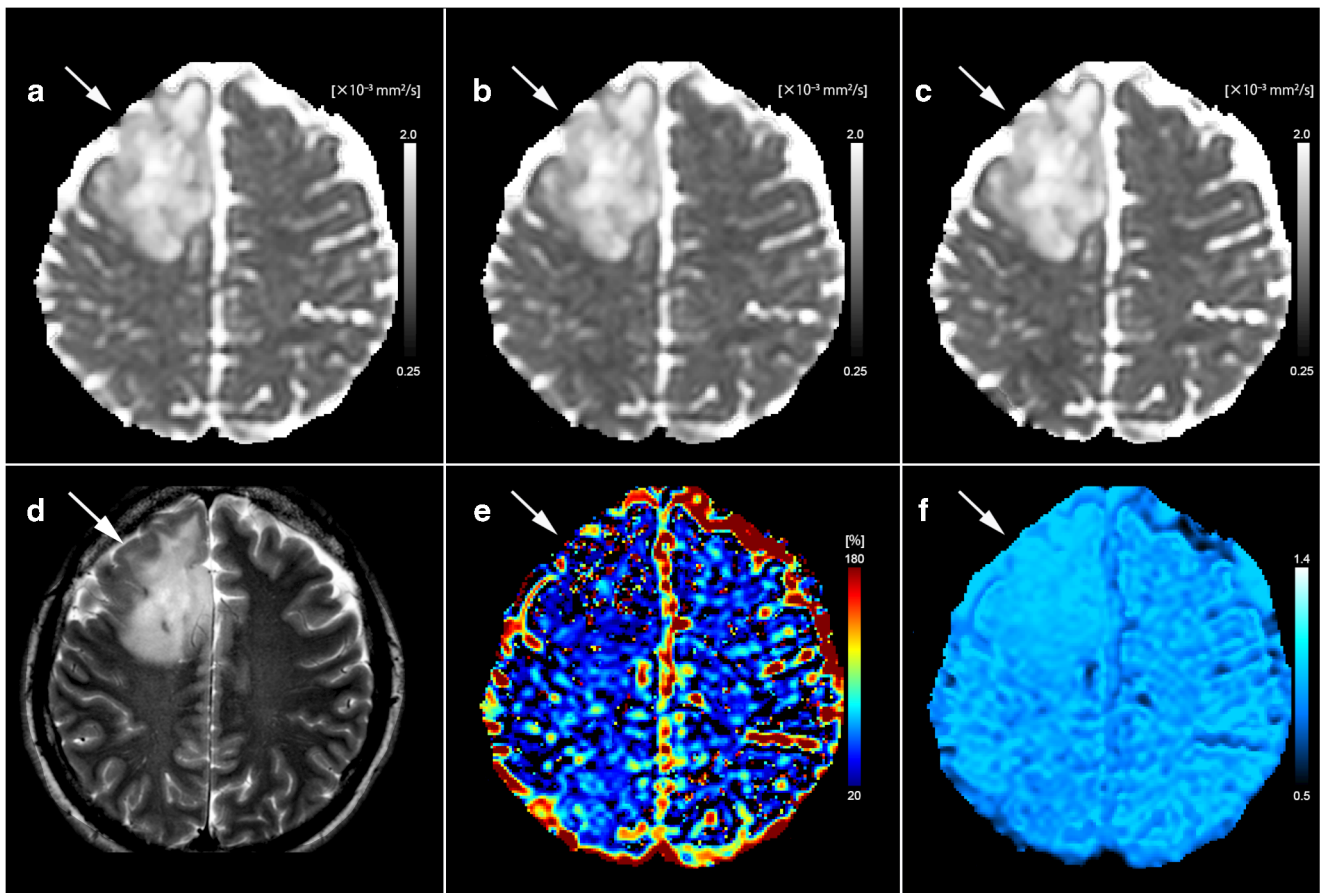


Fig. 3 Images from a 49-year-old woman with histologically proven oligodendroglioma, IDH-mutant type (WHO grade II). Diffusion-related coefficient maps show a heterogeneous mass of high values (**a** ADC map, **b** D map, **c** DDC map; $1.04, 1.00, 1.05 \times 10^{-3} \text{ mm}^2/\text{s}$, respectively) in the right frontal lobe (arrows). **d** The T2-weighted image shows

heterogeneously hyperintense mass. **e** The f map shows a low value (6.2%) in the lesion. **f** α map shows a high value (0.89) in the lesion. α heterogeneity index, ADC apparent diffusion coefficient, D true-diffusion coefficient, DDC distributed diffusion coefficient, f perfusion fraction, IDH isocitrate dehydrogenase, WHO World Health Organization

α_{10} was lower than that for the combined D10 and f90, it achieved a good diagnostic performance. The stretched-exponential model enables the simultaneous measurement of diffusion and heterogeneity. Other tumors with different histological features would show different patterns of diffusion, vascularity, and heterogeneity. It would be useful to assess which model is most effective for differentiating tumor malignancies.

This study has some limitations. First, the number of patients was small. Moreover, we matched the number of patients with HGGs and LGGs for statistical simplicity in this pilot study based on preliminary data. It would be desirable to proceed with a subsequent study with a larger number of patients. Second, the study design was retrospective in nature; thus, a patient selection bias could not be completely eliminated. Third, we did not evaluate b -values $> 1000 \text{ s}/\text{mm}^2$ in the measurements, which is unlike previous studies; however, an optimal upper b -value limit for brain tumors has not been determined. Fourth, we did not include the whole tumor volume in the histogram analysis. Instead, we used the maximum

section of the glioma, with its boundary defined by hyperintensity on T2-weighted images. However, in a previous study, whole-volume histogram analysis did not yield more accurate results than single-slice methods and took longer to complete [37]. In the ROI analysis, edematous or necrotic regions were included. However, identifying these regions would be a subjective process. Instead, we employed a histogram analysis with ROIs of all T2-prolonged areas of each tumor, which we believe is a more objective method, in the current study.

Conclusions

The mono-, bi-, and stretched-exponential DWI models provided useful imaging biomarkers related to essential histological features for the differentiation of gliomas using histogram analysis. In particular, the bi-exponential model exhibited the best diagnostic performance for differentiating HGGs from LGGs either by

evaluation of the perfusion parameter or both the diffusion and perfusion parameters simultaneously, thereby providing a helpful noninvasive diagnostic method for grading gliomas.

Acknowledgments This study was funded by a grant from the Clinical Research Promotion Foundation (2019). This work was supported by SPS KAKENHI Grant Number 20K16791, Grant of The Clinical Research Promotion Foundation (2019), foundation juridical person Kaibara Morikazu Medical Science Promotion Foundation, and Kawano Masanori Memorial Public Interest Incorporated Foundation for Promotion of Pediatrics.

Funding information This study was funded by a grant from the Clinical Research Promotion Foundation (2019). This work was supported by SPS KAKENHI Grant Number 20K16791, Grant of The Clinical Research Promotion Foundation (2019), foundation juridical person Kaibara Morikazu Medical Science Promotion Foundation, and Kawano Masanori Memorial Public Interest Incorporated Foundation for Promotion of Pediatrics.

Compliance with ethical standards

Conflict of interest We declare that we have no conflict of interest.

Ethical approval This retrospective study was approved by our Institutional Review Board.

Informed consent The requirement for informed consent was waived.

Open Access This article is licensed under a Creative Commons Attribution 4.0 International License, which permits use, sharing, adaptation, distribution and reproduction in any medium or format, as long as you give appropriate credit to the original author(s) and the source, provide a link to the Creative Commons licence, and indicate if changes were made. The images or other third party material in this article are included in the article's Creative Commons licence, unless indicated otherwise in a credit line to the material. If material is not included in the article's Creative Commons licence and your intended use is not permitted by statutory regulation or exceeds the permitted use, you will need to obtain permission directly from the copyright holder. To view a copy of this licence, visit <http://creativecommons.org/licenses/by/4.0/>.

References

- Louis DN, Perry A, Reifenberger G, von Deimling A, Figarella-Branger D, Cavenee WK, Ohgaki H, Wiestler OD, Kleihues P, Ellison DW (2016) The 2016 World Health Organization classification of tumors of the central nervous system: a summary. *Acta Neuropathol* 131:803–820. <https://doi.org/10.1007/s00401-016-1545-1>
- Stupp R, Mason WP, van den Bent MJ, Weller M, Fisher B, Taphoorn MJ, Belanger K, Brandes AA, Marosi C, Bogdahn U, Curschmann J, Janzer RC, Ludwin SK, Gorlia T, Allgeier A, Lacombe D, Cairncross JG, Eisenhauer E, Mirimanoff RO, European Organisation for Research and Treatment of Cancer Brain Tumor and Radiotherapy Groups, National Cancer Institute of Canada Clinical Trials Group (2005) Radiotherapy plus concomitant and adjuvant temozolomide for glioblastoma. *N Engl J Med* 352:987–996. <https://doi.org/10.1056/NEJMoa043330>
- Sugahara T, Korogi Y, Kochi M, Ikushima I, Shigematu Y, Hirai T, Okuda T, Liang L, Ge Y, Komohara Y, Ushio Y, Takahashi M (1999) Usefulness of diffusion-weighted MRI with echo-planar technique in the evaluation of cellularity in gliomas. *J Magn Reson Imaging* 9:53–60. [https://doi.org/10.1002/\(sici\)1522-2586\(199901\)9:1%3C53::aid-jmri7%3E3.0.co;2-2](https://doi.org/10.1002/(sici)1522-2586(199901)9:1%3C53::aid-jmri7%3E3.0.co;2-2)
- Server A, Kulle B, Gadmar OB, Josefsen R, Kumar T, Nakstad PH (2011) Measurements of diagnostic examination performance using quantitative apparent diffusion coefficient and proton MR spectroscopic imaging in the preoperative evaluation of tumor grade in cerebral gliomas. *Eur J Radiol* 80:462–470. <https://doi.org/10.1016/j.ejrad.2010.07.017>
- Lam WW, Poon WS, Metreweli C (2002) Diffusion MR imaging in glioma: does it have any role in the pre-operation determination of grading of glioma? *Clin Radiol* 57:219–225. <https://doi.org/10.1053/crad.2001.0741>
- Le Bihan D, Breton E, Lallemand D et al (1988) Separation of diffusion and perfusion in intravoxel incoherent motion MR imaging. *Radiology* 168:497–505. <https://doi.org/10.1148/radiology.168.2.3393671>
- Bisdas S, Koh TS, Roder C, Braun C, Schittenhelm J, Ernemann U, Klose U (2013) Intravoxel incoherent motion diffusion-weighted MR imaging of gliomas: feasibility of the method and initial results. *Neuroradiology* 55:1189–1196. <https://doi.org/10.1007/s00234-013-1229-7>
- Togao O, Hiwatashi A, Yamashita K, Kikuchi K, Mizoguchi M, Yoshimoto K, Suzuki SO, Iwaki T, Obara M, van Cauteren M, Honda H (2016) Differentiation of high-grade and low-grade diffuse gliomas by intravoxel incoherent motion MR imaging. *Neuro-Oncology* 18:132–141. <https://doi.org/10.1093/neuonc/nov147>
- Kikuchi K, Hiwatashi A, Togao O, Yamashita K, Kamei R, Momosaka D, Hata N, Iihara K, Suzuki SO, Iwaki T, Honda H (2019) Intravoxel incoherent motion MR imaging of pediatric intracranial tumors: correlation with histology and diagnostic utility. *AJNR Am J Neuroradiol* 40:878–884. <https://doi.org/10.3174/ajnr.A6052>
- Bennett KM, Schmainda KM, Bennett RT et al (2003) Characterization of continuously distributed cortical water diffusion rates with a stretched-exponential model. *Magn Reson Med* 50:727–734. <https://doi.org/10.1002/mrm.10581>
- Kwee TC, Galban CJ, Tsien C et al (2010) Intravoxel water diffusion heterogeneity imaging of human high-grade gliomas. *NMR Biomed* 23:179–187. <https://doi.org/10.1002/nbm.1441>
- Kwee TC, Galban CJ, Tsien C et al (2010) Comparison of apparent diffusion coefficients and distributed diffusion coefficients in high-grade gliomas. *J Magn Reson Imaging* 31:531–537. <https://doi.org/10.1002/jmri.22070>
- Bai Y, Lin Y, Tian J, Shi D, Cheng J, Haacke EM, Hong X, Ma B, Zhou J, Wang M (2016) Grading of gliomas by using monoexponential, biexponential, and stretched exponential diffusion-weighted MR imaging and diffusion kurtosis MR imaging. *Radiology* 278:496–504. <https://doi.org/10.1148/radiol.2015142173>
- Yan R, Haopeng P, Xiaoyuan F, Jinsong W, Jiawen Z, Chengjun Y, Tianming Q, Ji X, Mao S, Yueyue D, Yong Z, Jianfeng L, Zhenwei Y (2016) Non-Gaussian diffusion MR imaging of glioma: comparisons of multiple diffusion parameters and correlation with histologic grade and MIB-1 (Ki-67 labeling) index. *Neuroradiology* 58:121–132. <https://doi.org/10.1007/s00234-015-1606-5>
- Chakhoyan A, Woodworth DC, Harris RJ, Lai A, Nghiemphu PL, Liau LM, Pope WB, Cloughesy TF, Ellingson BM (2018) Monoexponential, diffusion kurtosis and stretched exponential diffusion MR imaging response to chemoradiation in newly diagnosed glioblastoma. *J Neuro-Oncol* 139:651–659. <https://doi.org/10.1007/s11060-018-2910-9>

16. Chen X, Jiang J, Shen N, Zhao L, Zhang J, Qin Y, Zhang S, Li L, Zhu W (2018) Stretched-exponential model diffusion-weighted imaging as a potential imaging marker in preoperative grading and assessment of proliferative activity of gliomas. *Am J Transl Res* 10:2659–2668
17. Liu C, Wang K, Li X, Zhang J, Ding J, Spuhler K, Duong T, Liang C, Huang C (2018) Breast lesion characterization using whole-lesion histogram analysis with stretched-exponential diffusion model. *J Magn Reson Imaging* 47:1701–1710. <https://doi.org/10.1002/jmri.25904>
18. Klaassen R, Gurney-Champion OJ, Engelbrecht MRW, Stoker J, Wilmink JW, Besselink MG, Bel A, van Tienhoven G, van Laarhoven HWM, Nederveen AJ (2018) Evaluation of six diffusion-weighted MRI models for assessing effects of neoadjuvant chemoradiation in pancreatic cancer patients. *Int J Radiat Oncol Biol Phys* 102:1052–1062. <https://doi.org/10.1016/j.ijrobp.2018.04.064>
19. Hu Y, Tang H, Li H, Li A, Li J, Hu D, Li Z, Kamel IR (2018) Assessment of different mathematical models for diffusion-weighted imaging as quantitative biomarkers for differentiating benign from malignant solid hepatic lesions. *Cancer Med*. <https://doi.org/10.1002/cam4.1535>
20. Mazaheri Y, Afaq A, Rowe DB et al (2012) Diffusion-weighted magnetic resonance imaging of the prostate: improved robustness with stretched exponential modeling. *J Comput Assist Tomogr* 36:695–703. <https://doi.org/10.1002/cam4.1535>
21. Wang Y, Hu D, Yu H, Shen Y, Tang H, Kamel IR, Li Z (2019) Comparison of the diagnostic value of monoexponential, biexponential, and stretched exponential diffusion-weighted MRI in differentiating tumor stage and histological grade of bladder cancer. *Acad Radiol* 26:239–246. <https://doi.org/10.1016/j.acra.2018.04.016>
22. Li H, Liang L, Li A, Hu Y, Hu D, Li Z, Kamel IR (2017) Monoexponential, biexponential, and stretched exponential diffusion-weighted imaging models: quantitative biomarkers for differentiating renal clear cell carcinoma and minimal fat angiomyolipoma. *J Magn Reson Imaging* 46:240–247. <https://doi.org/10.1002/jmri.25524>
23. Law M, Young R, Babb J et al (2007) Histogram analysis versus region of interest analysis of dynamic susceptibility contrast perfusion MR imaging data in the grading of cerebral gliomas. *AJNR Am J Neuroradiol* 28:761–766
24. Kang Y, Choi SH, Kim YJ, Kim KG, Sohn CH, Kim JH, Yun TJ, Chang KH (2011) Gliomas: histogram analysis of apparent diffusion coefficient maps with standard- or high-b-value diffusion-weighted MR imaging—correlation with tumor grade. *Radiology* 261:882–890. <https://doi.org/10.1148/radiol.11110686>
25. Seo N, Chung YE, Park YN, Kim E, Hwang J, Kim MJ (2018) Liver fibrosis: stretched exponential model outperforms monoexponential and bi-exponential models of diffusion-weighted MRI. *Eur Radiol* 28:2812–2822. <https://doi.org/10.1007/s00330-017-5292-z>
26. DeLong ER, DeLong DM, Clarke-Pearson DL (1988) Comparing the areas under two or more correlated receiver operating characteristic curves: a nonparametric approach. *Biometrics* 44:837–845
27. Lyng H, Haraldseth O, Rofstad EK (2000) Measurement of cell density and necrotic fraction in human melanoma xenografts by diffusion weighted magnetic resonance imaging. *Magn Reson Med* 43:828–836. [https://doi.org/10.1002/1522-2594\(200006\)43:6%3C828::aid-mrm8%3E3.0.co;2-p](https://doi.org/10.1002/1522-2594(200006)43:6%3C828::aid-mrm8%3E3.0.co;2-p)
28. Chen L, Liu M, Bao J, Xia Y, Zhang J, Zhang L, Huang X, Wang J (2013) The correlation between apparent diffusion coefficient and tumor cellularity in patients: a meta-analysis. *PLoS One* 8:e79008. <https://doi.org/10.1371/journal.pone.0079008>
29. Hilario A, Ramos A, Perez-Nunez A et al (2012) The added value of apparent diffusion coefficient to cerebral blood volume in the preoperative grading of diffuse gliomas. *AJNR Am J Neuroradiol* 33:701–707. <https://doi.org/10.3174/ajnr.A2846>
30. Lee EJ, Lee SK, Agid R, Bae JM, Keller A, terBrugge K (2008) Preoperative grading of presumptive low-grade astrocytomas on MR imaging: diagnostic value of minimum apparent diffusion coefficient. *AJNR Am J Neuroradiol* 29:1872–1877. <https://doi.org/10.3174/ajnr.A1254>
31. Kim HS, Kim SY (2007) A prospective study on the added value of pulsed arterial spin-labeling and apparent diffusion coefficients in the grading of gliomas. *AJNR Am J Neuroradiol* 28:1693–1699. <https://doi.org/10.3174/ajnr.A0674>
32. King AD, Chow KK, Yu KH, Mo FKF, Yeung DKW, Yuan J, Bhatia KS, Vlantis AC, Ahuja AT (2013) Head and neck squamous cell carcinoma: diagnostic performance of diffusion-weighted MR imaging for the prediction of treatment response. *Radiology* 266:531–538. <https://doi.org/10.1148/radiol.12120167>
33. Yamashita K, Hiwatashi A, Togao O, Kikuchi K, Kitamura Y, Mizoguchi M, Yoshimoto K, Kuga D, Suzuki SO, Baba S, Isoda T, Iwaki T, Iihara K, Honda H (2016) Diagnostic utility of intravoxel incoherent motion MR imaging in differentiating primary central nervous system lymphoma from glioblastoma multiforme. *J Magn Reson Imaging* 44:1256–1261. <https://doi.org/10.1002/jmri.25261>
34. Federau C, Hagmann P, Maeder P, Müller M, Meuli R, Stuber M, O'Brien K (2013) Dependence of brain intravoxel incoherent motion perfusion parameters on the cardiac cycle. *PLoS One* 8:e72856. <https://doi.org/10.1371/journal.pone.0072856>
35. Habib J, Auer DP, Morgan PS (2010) A quantitative analysis of the benefits of cardiac gating in practical diffusion tensor imaging of the brain. *Magn Reson Med* 63:1098–1103. <https://doi.org/10.1002/nrm.22232>
36. Federau C, Meuli R, O'Brien K, Maeder P, Hagmann P (2014) Perfusion measurement in brain gliomas with intravoxel incoherent motion MRI. *AJNR Am J Neuroradiol* 35:256–262. <https://doi.org/10.3174/ajnr.A3686>
37. Han X, Suo S, Sun Y, Zu J, Qu J, Zhou Y, Chen Z, Xu J (2017) Apparent diffusion coefficient measurement in glioma: influence of region-of-interest determination methods on apparent diffusion coefficient values, interobserver variability, time efficiency, and diagnostic ability. *J Magn Reson Imaging* 45:722–730. <https://doi.org/10.1002/jmri.25405>

Publisher's note Springer Nature remains neutral with regard to jurisdictional claims in published maps and institutional affiliations.